Intelligent Control of DFIG Using Sensorless Speed Estimation and Lookup Table-Based MPPT Algorithm to Overcome Wind and Grid Disturbances

D.V.N. Ananth and G.V. Nagesh Kumar

Abstract Doubly fed induction generator (DFIG) needs to get adapted to situations like rapid change in wind speed and sudden requirement for grid disturbances to meet modern grid rules. The paper explains the design of controllers for MPPT algorithm for the turbine, DFIG converters, and sensorless rotor speed estimation. These intelligent controllers are used to maintain equilibrium in rotor speed, generator torque, and stator and rotor voltages. They are also designed to meet desired reference real and reactive power during the turbulences like sudden change in reactive power or voltage with concurrently changing wind speed. The turbine blade angle changes with variations in wind speed and direction of wind flow and improves the coefficient of power extracted from turbine using MPPT algorithm. Rotor side converter (RSC) helps to achieve optimal real and reactive power from generator, which keeps rotor to rotate at optimal speed and to vary current flow from rotor and stator terminals. For tracking reactive power demand from grid and in maintaining synchronism when grid voltage changes due to fault at a very faster and stable way Grid side converter (GSC) is helpful. Rotor speed is estimated using stator and rotor flux estimation algorithm. Parameters like stator and rotor voltage, current, real, reactive power, rotor speed, and electromagnetic torque are studied using MATLAB simulation. The performance of DFIG is compared when there is in wind speed change only; alter in reactive power and variation in grid voltage individually along with variation in wind speed.

Keywords Doubly fed induction generator · MPPT algorithm · Reactive power control · Rotor speed estimation

D.V.N. Ananth
VITAM College of Engineering, Visakhapatnam, India

G.V. Nagesh Kumar (✉)
GITAM University, Visakhapatnam, India
e-mail: gundavarapu_kumar@yahoo.com

1 Introduction

Renewable energy resources like wind and solar electric power generation systems are getting significance due to retreating of primary fuels and eco-friendly nature and are available from few kilo-watt powers to megawatt rating and the back-to-back converters are rated from 25 to 35 % of generator stator rating [1]. Capability to extract more or maximum power point tracking theorem (MPPT) [2], The DFIG is getting importance compared to permanent magnet synchronous generator (PMSG) or asynchronous generator because of operation under variable speed conditions [3–5], effective performance during unbalanced and flickering loads [6].

Maximum power extraction from DFIG using pitch angle controller and optimal power coefficient at low and high speed is analyzed in [7]. Direct and indirect control of reactive power control with an aim to meet active and reactive power equal to the reference values as achieved in [8]. MPPT-based WECs design facilitates the wind turbine has to operate in variable speed as per the ideal cube law power curve [9–13]. The constant power mode of operation can be achieved by (i) including energy storage devices [13–17] and (ii) employing pitch control [9, 18, 19].

In this paper, performance of DFIG was compared and analyzed under situations like, with variation in wind speed alone, with reactive power variation and with grid voltage variation for same variation in wind speed. In these cases, variation in tip speed ratio and coefficient of turbine power, effect on real and reactive power flows, voltages and current from stator, rotor, rotor speed and electromagnetic torque are examined. The paper was organized with overview of WECS with wind turbine modeling and pitch angle controller in Sect. 2, study of mathematical modeling of DFIG in Sect. 3, the Sect. 4 describe RSC architecture and design; Sect. 5 analyses the performance of DFIG for three cases like effect of variation on wind speed variation, reactive power demand along with variation in wind speed and grid voltage variation with wind speed. Conclusion was given in Sect. 6. System parameters are given in "Appendix".

2 Wind Energy Conversion Systems (WECS)

The wind turbine is the prime mover which facilitates in converting kinetic energy of wind into mechanical energy which further converted into electrical energy.

2.1 Pitch Angle Controller

The wind turbine blade angles are controlled by using servo mechanism to maximize turbine output mechanical power during steady state and to protect the turbine during high wind speeds. This control mechanism is known as pitch angle
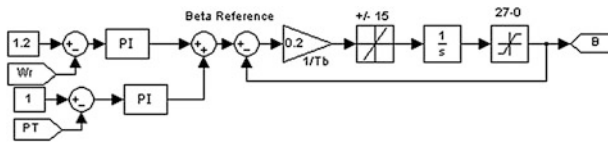
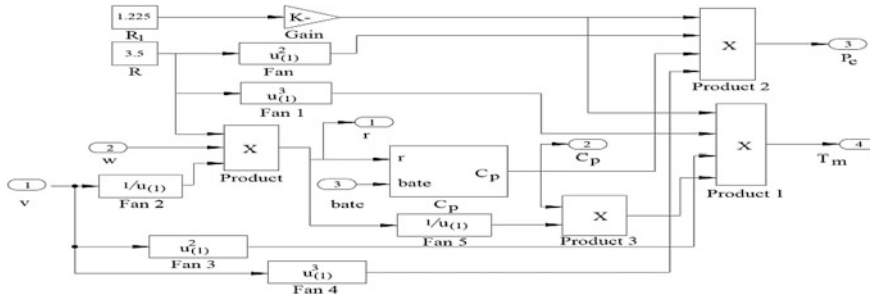**Fig. 1** Pitch angle controller design for wind turbine

Fig. 2 Reference electrical power generation control circuit and mechanical torque output from turbine with MPPT algorithm

controller. When wind speed is at cut-in speed, the blade pitch angle is set to produce optimal power, at rated wind speed; it is set to produce rated output power from generator. At higher wind speeds, this angle increases and makes the turbine to protect from over-speeding.

In this system reference generator speed is $W_r^{ref} = 1.2$ pu or is obtained from MPPT algorithm and actual speed of the generator is Wr. The actual speed can be estimated using an encoder or using sensorless estimation strategy. The error between reference and actual values is controlled using PI controller. In the similar way, the difference in reference (P* = 1) and actual power outputs from turbine (PT) is controlled by PI controller. Both the outputs from PI controller are designed to get reference pitch angle controller (βref). The closed loop control of pitch angle is obtained as shown in Fig. 1.

The reference real power (Pe) or actual mechanical output from turbine and mechanical output torque (Tm) is shown in Fig. 2. Using Tip Speed Ratio (TSR) and Coefficient of Power (Cp) are used to generate reference power and the control scheme is useful to extract maximum mechanical power, thereby more mechanical tore Tm by using the MPPT algorithm. The aim of MPPT algorithm is to generate optimal mechanical power output from turbine and mechanical input torque to give to doubly fed induction generator. The mechanical power is given as reference to grid side converter (GSC) to make the rotor to rotate at optimal speed. The optimal input torque to DFIG is so as to operate for extracting maximum power from the generator.

The inputs to MPPT algorithm are radius of curvature 'R' of turbine wings, rotor speed (Wr), wind sped (V_w), and pitch angle (beta). Initially with R, W_r, and Vw, tip speed ratio (g) is determined. Later using Eq. 2 and input parameter beta, coefficient of power (Cp) is calculated. Based on Eq. 5, optimal mechanical power (P_{m_opt}) is determined and dividing mechanical power by rotor speed, optimal torque (T_{m_opt}) is determined. The pitch angle (beta) is determined as shown in Fig. 2. The application of P_{m_opt} and T_{m_opt} is shown in Figs. 4 and 5. Optimal real power generation is achieved by extracting optimal mechanical power output from turbine when made to run at optimal loading and speed. For this MPPT algorithm proposed will be very helpful.

2.2 Mathematical Modeling of DFIG

The equivalent circuit of DFIG in rotating reference frame at an arbitrary reference speed of ω is shown in Fig. 3. The equations can be derived in dq reference frame were as follows:

The rotor direct and quadrature axis are derives as

$$V_{rd} = R_r I_{rd} - (\omega_s - \omega_r)\psi_{rq} + \frac{d\psi_{rd}}{dt} \tag{1}$$

$$V_{rq} = R_r I_{rq} + (\omega_s - \omega_r)\psi_{rd} + \frac{d\psi_{rq}}{dt} \tag{2}$$

The difference between stator speed (ω_s) and rotor speed (ω_r) is known as slip speed ($s\omega_s$). For motoring action, this difference is less than zero and for generating, the slip speed is negative.

The stator real power in terms of two axis voltage and current is

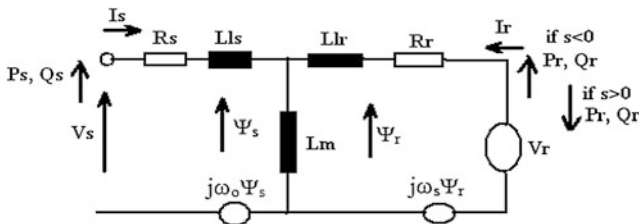$$P_s = \frac{3}{2} \left(V_{sd}I_{sd} + V_{sq}I_{sq}\right) \tag{3}$$

Fig. 3 Equivalent circuit of DFIG in rotating reference frame at speed ω

The rotor real power in terms of two axis voltage and current is

$$P_r = \frac{3}{2} \left(V_{rd}I_{rd} + V_{rq}I_{rq} \right) \tag{4}$$

The stator reactive power in terms of two axis voltage and current is

$$Q_s = \frac{3}{2} \left(V_{sq}I_{sd} - V_{sd}I_{sq} \right) \tag{5}$$

The rotor reactive power in terms of two axis voltage and current is

$$Q_r = \frac{3}{2} \left(V_{rq}I_{rd} - V_{rd}I_{rq} \right) \tag{6}$$

The output electromagnetic torque is given by the equation

$$T_e = \frac{3}{2} pL_m \left(I_{sq}I_{rd} - I_{sd}I_{rq} \right) \tag{7}$$

3 Rotor Side Controller (RSC) and Grid Side Controller (GSC) Architecture and Design

3.1 Operation of GSC and RSC Controllers

The rotor side converter (RSC) is used to control the speed of rotor and also helps in maintaining desired grid voltage as demanded. The control circuit for grid side controller (GSC) is shown in Fig. 4 and rotor side controller (RSC) is shown in Fig. 5 with internal circuits for deriving RSC PLL for 2–3 phases inverse Parks transformation is shown in Fig. 6. This Fig. 6 helps to inject current in rotor winding at slip frequency. The GSC and RSC have four control loops each, later has one speed control loop, other is reactive power and last two are direct and quadrature axis current control loops. The speed and reactive power control loops are called outer control loop and direct and quadrature axis control loops are called inner control loops.

The reference rotor speed is derived from the wind turbine optimal power output P_{mOpt} as shown in Fig. 4 and grid power demand. In total, the reference power input to the lookup table as shown in Fig. 5 is $P_{m,gOpt}$. Based on the value of $P_{m,gOpt}$, the rotor is made to rotate at optimal speed so as to extract maximum power from DFIG set. The difference between reference speed of generator and actual speed of generator is said to be rotor speed error. Speed error is minimized and maintained nearly at zero value by using speed controller loop which is a PI controller with K_{pn} and K_{in} as proportional and integral gain parameters. The output from speed controller is
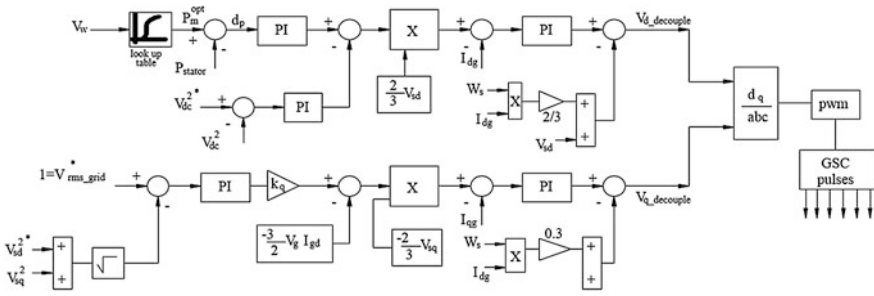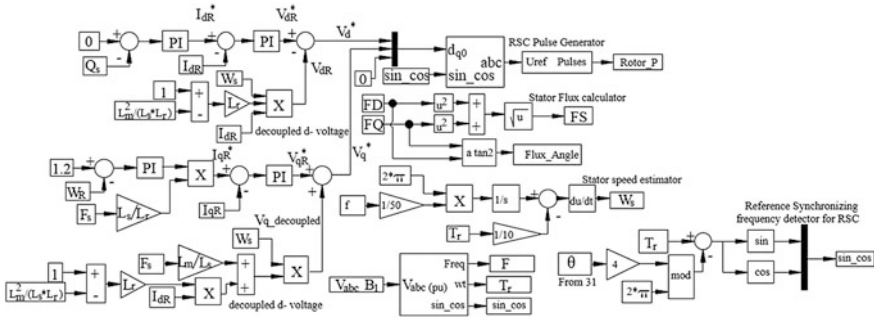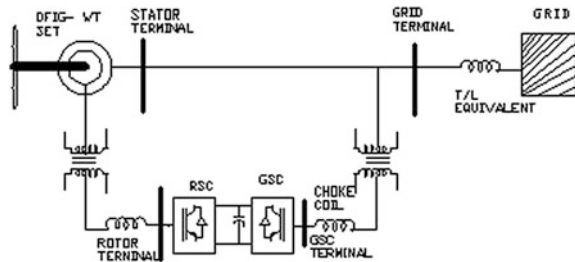
Fig. 4 Grid side controller for DFIG

Fig. 5 Rotor side controller for DFIG

Fig. 6 Design of overall DFIG system with RSC and GSC

multiplied with stator flux (F_s) and ratio of stator and rotor (L_s and L_r) inductances to get reference quadrature current (I_{qr}) for rotor. The error in reference and actual reactive power give reference direct axis current (I_{qr}). The difference between these reference and actual two axis currents is controlled by tuned PI controller to get respective direct and quadrature axis voltages. The output from each PI controller is manipulated with disturbance voltages to get reference voltage for pulse generation as shown in Fig. 5. It must be noted that the pulses are regulated at slip frequency for RSC rather than at fundamental frequency and slip frequency synchronizing for inverse Park's transformation can also be seen in the figure.

The block diagram of GSC is shown in Fig. 4. For a given wind speed, reference or control power from turbine is estimated using lookup table. From Eq. (3), stator real power (P_{stator}) is calculated and the error in powers is difference between these two powers (dP) which is to be maintained near zero by PI controller. The output from PI controller is multiplied with real power constant (K_p) gives actual controllable power after disturbance. The difference in square of reference voltage across capacitor dc link (V_{dc}^*) and square of actual dc link voltage (V_{dc}) is controlled using PI controller to get reference controllable real power. The error in the reference and actual controllable power is divided by using $2/3V_{sd}$ to get direct axis (d-axis) reference current near grid terminal (Igdref). Difference in Igdref and actual d-axis grid current is controlled by PI controller to get d-axis voltage. But to achieve better response during transient conditions, decoupling d-axis voltage is added as in case of separately excited DC motor. This decoupling term helps in controlling steady state error and fastens transient response of DFIG during low voltage ride through (LVRT) or during sudden changes in real or reactive powers from/to the system.

Similarly from stator RMS voltage (V_s) or reference reactive power, actual stator voltage or reactive power is subtracted by PI controller and multiplied with appropriate reactive power constant (K_q) to get actual reference reactive power compensating parameter. From Eq. (5), actual reactive power is calculated and the difference in this and actual compensating reactive power and when divided by $2/3Vsq$, we get quadrature axis (q-axis) reference current (I_{qref}). When the difference in I_{qref} and stator actual q-axis current (I_q) is controlled by PI controller, reference q-axis voltage is obtained. As said earlier, to improve transient response and to control steady state error, decoupled q-axis voltage has to be added as shown in Fig. 4. Both d- and q- axis voltage parameters so obtained are converted to three axis abc parameters by using inverse Park's transformation and reference voltage is given to scalar PWM controller to get pulses for grid side controller. The DFIG grid connected system general layout is shown in Fig. 6.

The rotating direct and quadrature reference voltages of rotor are converted into stationary abc frame parameters by using inverse parks transformation. Slip frequency is used to generate sinusoidal and cosine parameters for inverse parks transformation.

3.2 Rotor Speed Sensing by Using Sensorless Control Technique

The sensorless speed control for DFIG system with stator and rotor flux observers are shown in Fig. 7. The internal sub-systems to produce two axis qauadrature and direct axis flux is given in Fig. 8a, b. The three phase stator voltage and currents are converted into two phase dq voltages and current by using Park's transformation. The dq axis stator voltage and current are transformed into dq axis stator flux based
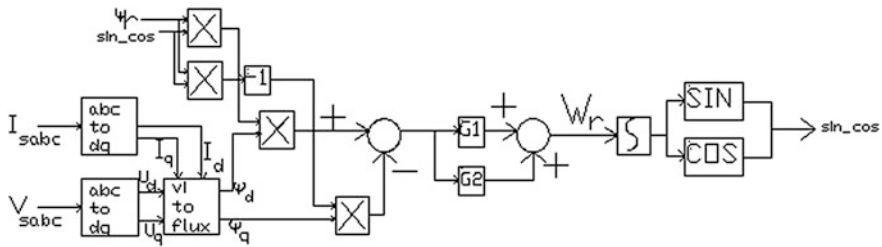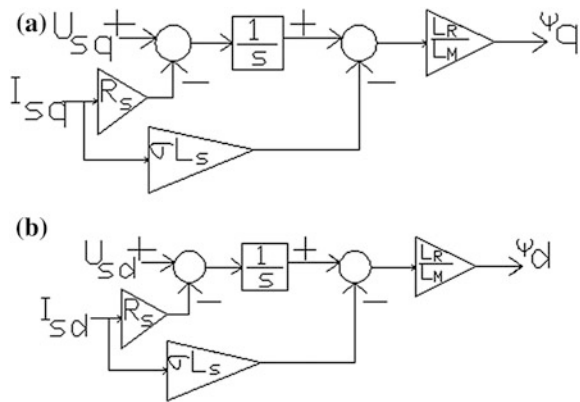
Fig. 7 Estimation of rotor speed with stator voltage and current and rotor flux as inputs

Fig. 8 a Derivation of stator
q-axis flux from q-axis stator
voltage and current Eq. 2.
b Derivation of stator d-axis
flux from d-axis stator voltage
and current from Eq. 1

on Eqs. 1 and 2. The internal structure for dq axis flux derivations are shown in
Fig. 8a, b.

The derived rotor and stator flux are compared and is controlled to estimate rotor
speed by using PI controller. The blocks G1 and G2 are PI controller functional
blocks. The speed is estimated and is termed as W_r and is integrated to get rotor
angle. The angle is multiplied with trigonometric SIN and COS terms and is given
to mux to get sin_cos parameters and the total setup can be used as phase locked
loop (PLL). This sin_cos helps in estimating exact phase sequence and for locking
the new system to reference grid. The estimated speed W_r is given as input for RSC
controller as shown in Fig. 5. From the lookup table, reference rotor speed is
estimated from optimal power block, which is obtained from MPPT algorithm.

4 Results and Discussion

The dynamic performance of the DFIG system as shown in Fig. 6 is investigated
with three different cases and rating specifications for DFIG and wind turbine
parameters are given in "Appendix". The wind speed change in all cases in meters

per seconds as 8, 15, 20, and 10 at 15, 25, and 35 s. The reactive power and voltage value change in individual two cases with change in time is from −0.6 pu at 12 s to 0 pu change at 20 s. It was further changed from 0 to +0.6 pu magnitude at 30 s. DFIG will become better generator source if immediately it can supply any desired reactive power effectively. The change in grid terminal voltage takes place when suddenly switching on or off large loads or due to small faults near point of common coupling (PCC). The effect of change in wind speed, change in wind speed with reactive power, and change in wind speed with grid terminal voltages on generator and turbine parameters are studied.

Case A: Change in TSR and C_p with wind speed, reactive power, and grid voltage

The changes in tip-speed ration and power coefficient C_p with change in wind speed alone is shown in Fig. 9(i), with both reactive power and wind speed variation in Fig. 9 (ii) and variation with grid terminal voltage and wind speed both is shown in Fig. 9(iii). It can be observed that when wind speed is at 8 m/s, tip speed ratio (TSR) is high near 4.8° and slowly decreases to 2.6° at 15 s when speed increases to 15 m/s, further increased to 1.9° at 25 s when speed of wind is 20 m/s and decreased to 3.9° when wind speed decreased to 10 m/s at 35 s. In the similar way, C_p is also changing from 3.25 to 1.7 at 15 s, and further decreased to 1.25 at 25 s, and then increased to 2.55 at 35 s with wind speed variation from 8 to 15 and then to 20, and 10 m/s. The variation in TSR and C_p with change in reactive power is independent and has no effect as shown in Fig. 9(i), (ii). However, with change in grid terminal voltage, a very small change in TSR and C_p can be observed. It is shown in Fig. 9(iii). It is due to the fact that the TSR and C_p depends on parameters as described by Eqs. 1–5 and is independent on voltage and reactive power. The TSR and C_p are blade size and shape with change in ambient temperature and wind speed dependant natural parameters.

To meet the desired grid reactive power, both stator and rotor has to supply for faster dynamics with an aid to RSC and GSC control schemes and is achieving as shown in Fig.9(ii). With the change in wind speed and reactive power, real power from generator is matching its reference value for case 2, but small deviation can be observed from time 30 to 35 s is due to sudden change in reactive power demand from grid and the deviation in real power is from 0.8 to 0.7 pu which is small. However, reactive power is following its trajectory within 1 s. In case 3, both voltage and reactive power changing with time, the deviation in real power and is following the trajectory nearly accurate with maximum deviation of 5 % in real power. The reactive power change with grid voltage is high when voltage decreased from 1 to 0.8 pu volts. When wind speed is increasing, mechanical and electrical torques are increasing without any change in stator reactive power.

Variation in grid reactive power causes quadrature currents on both stator and rotor to change but torque, speed or real powers from stator or rotor remains unaltered. The change in three cases is tabulated below. The variation in reactive power and grid voltage variations during the respective time period is shown in Tables 2 and 3. In Table 1, due to change in wind speed input to turbine alone, generator and wind turbine parameters change are summarized.
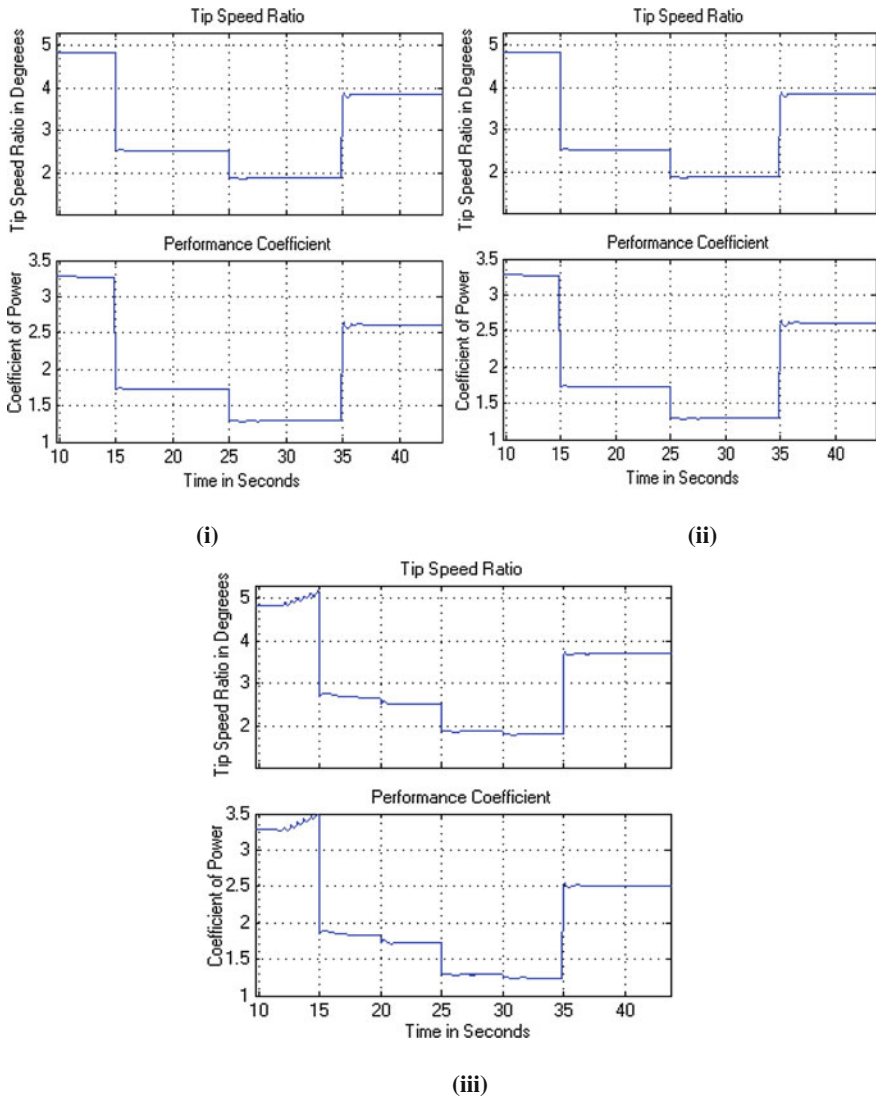
(i)   (ii)

(iii)

Fig. 9 Tip speed ratio and coefficient of power C_p for **i** change in wind speed alone, **ii** reactive power change and wind speed variation, **iii** both grid voltage and wind speed changes

Case B: Change in electromagnetic torque and rotor speed with wind speed, reactive power, and grid voltage

The reference mechanical turbine torque and generator torque with magnitudes overlapping and variation of rotor speed for all three cases comparison is shown in Fig. 10. In this the reference and actual torque waveform with blue color is turbine reference torque and pink color lines are for generator torque. It can be observed in

Table 1 Change in reactive power during the time period along with change in wind speed

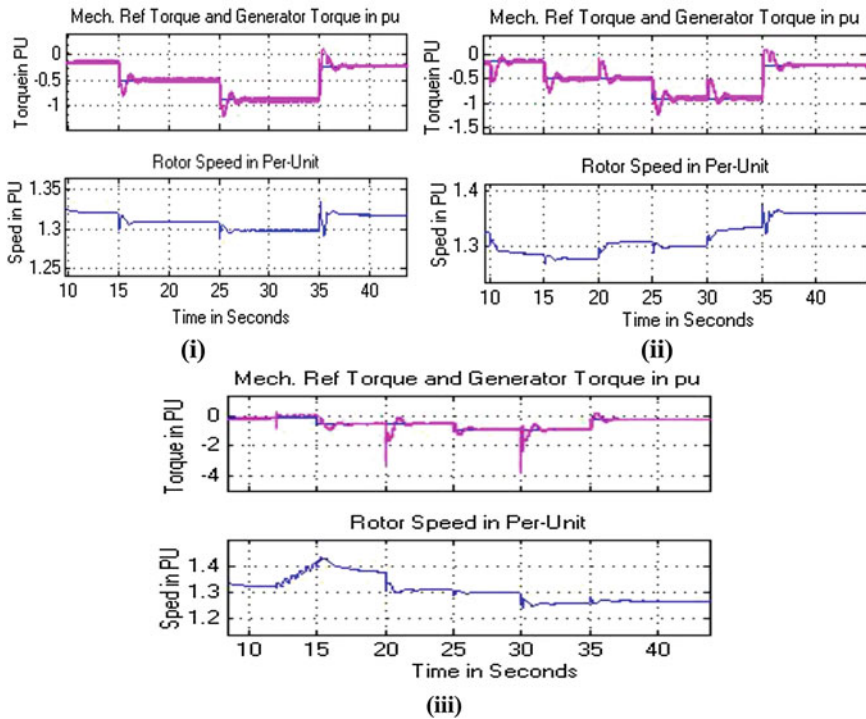| Time range (s)	0–20	20–30	30–50
Reactive power (pu)	−0.6	0	0.6

Fig. 10 Reference and actual generator torque and rotor for **i** change in wind speed, **ii** reactive power and wind speed variation, **iii** both grid voltage and wind speed changes

Fig. 10(i), (ii), and (iii), with increase in wind speed, torque is increasing and vice versa. Till time up to 15 s, wind speed is at low value of 8 m/s, so torque is at −0.2 pu and increased to −0.5 pu at 15 s with increase in wind speed to 15 m/s. The torque further increased to −0.9 pu when wind speed is 20 m/s and decreased to −0.28 pu when speed decreased to 10 m/s. There are small surges in torque waveform because of sudden change in wind speed.

In the first case, reactive power was at 0 pu and grid terminal voltage is 1 pu. The changes in torque have effect with change in reactive power as in Fig. 10(ii) and further more surges been observed when grid voltage disturbance occurred as in Fig. 10(iii) is taking place. When reactive power is lagging at −0.6 pu, there is a small surge in torque at 20 s. Generator speed is also low at 1.27 pu at −0.6 pu

reactive power, while at 0 pu reactive power, it is 1.32 pu speed. But rotor speed increased to 1.4 pu speed at low terminal grid voltage of 0.8 pu. When, reactive power changes to 0 pu from −0.6 pu, rotor speed increased to 1.3 pu from 1.27 pu and grid terminal voltage changes to 1 pu from 0.8 pu between 20 to 30 s. Speed further increased to 1.35 pu with leading reactive power of +0.6 pu and decreased when grid voltage increased from 1 to 1.2 pu. Therefore rotor speed increases if reactive power changes from lagging (−ve) to leading (+ve) and rotor speed decreases with increase in grid terminal voltage beyond 1 pu value in rms.

Case C: Comparison of reference and actual stator real and reactive power with change in wind speed, reactive power, and grid voltage

The reference mechanical power output is shown with pink line and generator power is with blue line for the first case is shown in Fig. 11(i). It can be observed that, nearly generator actual power is matching with reference power and the mismatch is because of looses in turbine, gear wheels and generator and this mismatch is inevitable. With increase in wind speed, reference power is increasing and vice versa. When wind speed is 8 ms, output electrical real power is 0.1 pu till 15 s and reaches 0.4 and 0.8 pu at 15 and 25 s with wind speed changing from 15 to 25 m/s and then decreases to 0.2 pu due to decrease in wind speed to 10 m/s, respectively. With the change in voltage at grid, stator terminal real power is maintained at constant value but with surges at instant of transient but reactive power is adjusting till stator voltage reaches the grid voltage for maintaining synchronism as shown in Fig. 11(iii). At the instant of 20 and 30 s, there is surge in real and reactive powers but were maintaining constant stator output real powers of 0.5 and 0.8 pu watts and 0 pu Var as in Fig. 11(ii).

To meet the desired grid reactive power, both stator and rotor has to supply for faster dynamics with an aid to RSC and GSC control schemes and is achieving as shown in Fig. 11(ii). With the change in wind speed and reactive power, real power from generator is matching its reference value for case 2, but small deviation can be observed from time 30 to 35 s is due to sudden change in reactive power demand from grid and the deviation in real power is from 0.8 to 0.7 pu which is small. However, reactive power is following its trajectory within 1 s. In the case 3, both voltage and reactive power changing with time, the deviation in real power and is following the trajectory nearly accurate with maximum deviation of 5 % in real power. The reactive power change with grid voltage is high when voltage decreased from 1 to 0.8 pu volts. When wind speed is increasing, mechanical and electrical torques are increasing without any change in stator reactive power.

Variation in grid reactive power causes quadrature currents on both stator and rotor to change but torque, speed or real powers from stator or rotor remains unaltered. The change in three cases is tabulated below. The variation in reactive power and grid voltage variations during the respective time period is shown in Tables 2 and 3. In Table 1, due to change in wind speed input to turbine alone, generator and wind turbine parameters change are summarized. There are surges
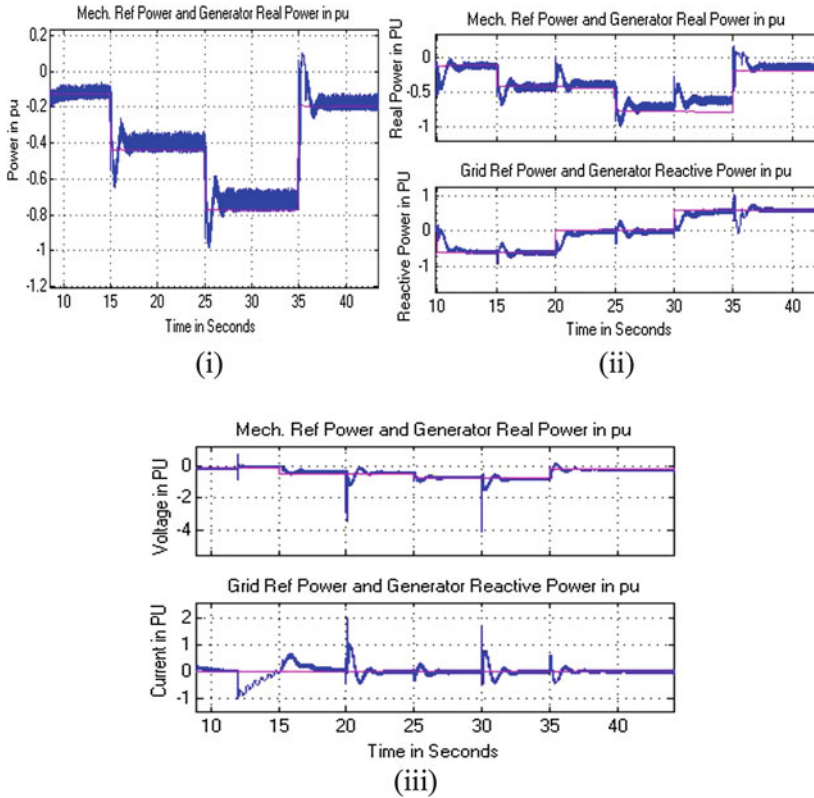
Fig. 11 Generator reference and actual real power waveform with time for **i** change in wind speed alone, generator real and reactive power flows for actual and reference for change in **ii** reactive power change and wind speed variation, **iii** both grid voltage and wind speed changes

Table 2 Change in grid voltage during the time period along with change in wind speed	Time range (s)	0–12	12–20	20–30	30–50
	Reactive power (pu)	1	0.8	1	1.2

produced in the electromagnetic torque (EMT) due to variations in reactive power and grid voltage. Large spikes in stator current and rotor current are produced due to sudden increase or decrease in grid voltage. Certain deviations in rotor speed can be observed due to change in reactive power or grid voltage. It is due to variation in current flow in the rotor circuit, thereby variation in rotor flux and hence rotor speed.

Table 3 Variation of turbine and generator parameters with change in wind speed input

Parameter variation with wind speed	Wind speed (m/s)			
	8	15	20	10
Time (s)	10	15	25	35
TSR (degree)	4.9	2.5	1.95	3.95
C_p	3.25	1.75	1.25	2.60
EMT (pu)	−0.2	−0.5	−0.8	−0.3
Rotor speed (pu)	1.32	1.31	1.30	1.33
Stator current (pu)	0.2	0.5	0.8	0.3
Rotor current (pu)	0.25	0.55	0.90	0.35
Stator power (pu)	−0.2	−0.5	−0.8	−0.3
Rotor power (pu)	0	0	0	0

5   Conclusions

From the proposed control scheme, the torque, speed, and reactive power control of DFIG is very specific. With change in wind speed, electromagnetic torque surges are low and the variation in wind speed is not getting the generator rotor speed variation is due to better transition in gear wheel mechanism. Reactive power demand from grid is accurate which can be met by proper control action of RSC and GSC. The proposed methodology is accurate and following all basic mathematical equations derived in this paper. Distinct from reactive power variation, change in voltage is not affecting any deviation in real power and is following the trajectory nearly accurate with maximum deviation of 5 % in real power. The reactive power change with grid voltage is high when voltage decreased from 1 to 0.8 pu volts. Hence the proposed control scheme can be applied with ever changing transients like large variation in wind speed, reactive power and grid voltage. The system is very stable without losing synchronism when grid voltage is increasing or decreasing to a ±0.2 pu change from nominal voltage value.

Appendix

The parameters of DFIG used in simulation are: Rated Power = 1.5 MW, Rated Voltage = 690 V, Stator Resistance Rs = 0.0049 pu, rotor Resistance Rr = 0.0049 pu, Stator Leakage Inductance Lls = 0.093 pu, Rotor Leakage inductance Llr1 = 0.1 pu, Inertia constant = 4.54 pu, Number of poles = 4, Mutual Inductance Lm = 3.39 pu, DC link Voltage = 415 V, Dc link capacitance = 0.2 F, Wind speed = 14 m/s. Grid Voltage = 25 kV, Grid frequency = 60 Hz. Grid side Filter: Rfg = 0.3 Ω, Lfg = 0.6 nH. Rotor side filter: Rfr = 0.3 mΩ, Lfr = 0.6 nH. Wind speed variations: 8, 15, 20 and 10 at 15, 25 and 35 s. Reactive power change: −0.6 to 0 and +0.6 pu at 20 and 30 s. Grid voltage change: 0.8–1 and to 1.2 pu at 20 and 30 s.

References

1. Aghanoori, N., Mohseni, M., Masoum, M.A.S.: Fuzzy approach for reactive power control of DFIG-based wind turbines. In: IEEE PES Innovative Smart Grid Technologies Asia (ISGT), pp: 1–6 (2011)
2. Kazmi, S.M., Goto, H., Guo, H.-J., Ichinokura, O.: A novel algorithm for fast and efficient speed-sensor less maximum power point tracking in wind energy conversion systems. IEEE Trans. Ind. Electron. **58**(1), 29–36 (2011)
3. Iwanski, G., Koczara, W.: DFIG-based power generation system with UPS function for variable-speed applications. IEEE Trans. Ind. Electron. **55**(8), 3047–3054 (2008)
4. Aktarujjaman, M., Haque, M.E., Muttaqi, K.M., Negnevitsky, M., Ledwich, G.: Control dynamics of a doubly fed induction generator under sub- and super-synchronous modes of operation. In: IEEE Power and Energy Society General Meeting—Conversion, and Delivery of Electrical Energy in the 21st Century, pp. 1–9 (2008)
5. Iwanski, G., Koczara, W.: DFIG-based power generation system with UPS function for variable-speed applications. IEEE Trans. Ind. Electron. **55**(8), 3047–3054 (2008)
6. Shukla, R.D., Tripathi, R.K.: Low voltage ride through (LVRT) ability of DFIG based wind energy conversion system II. In: Students Conference on Engineering and Systems (SCES), pp. 1–6 (2012)
7. Díaz, G.: Optimal primary reserve in DFIGs for frequency support. Int. Electr. Power Energy Syst. **43**, 1193–1195 (2012)
8. Poitiers, F., Bouaouiche, T., Machmoum, M.: Advanced control of a doubly-fed induction generator for wind energy conversion. Electr. Power Syst. Res. **79**, 1085–1096 (2009)
9. Cardenas, R., Pena, R., Perez, M., Clare, J., Asher, G., Wheeler, P.: Power smoothing using a flywheel driven by a switched reluctance machine. IEEE Trans. Ind. Electron. **53**(4), 1086–1093 (2006)
10. Muljadi, E., Butterfield, C.P.: Pitch-controlled variable-speed wind turbine generation. IEEE Trans. Ind. Appl. **37**(1), 240–246 (2001)
11. Wei, Q., Wei, Z., Aller, J.M., Harley, R.G.: Wind speed estimation based sensorless output maximization control for a wind turbine driving a DFIG. IEEE Trans. Power Electron. **23**(3), 1156–1169 (2008)
12. Sharma, S., Singh, B.: Control of permanent magnet synchronous generator-based stand-alone wind energy conversion system. IET Power Electron. **5**(8), 1519–1526 (2012)
13. Kazmi, S.M.R., Goto, H., Hai-Jiao, G., Ichinokura, O.: A novel algorithm for fast and efficient speed-sensorless maximum power point tracking in wind energy conversion systems. IEEE Trans. Ind. Electron. **58**(1), 29–36 (2011)
14. Mathiesen, B.V., Lund, H.: Comparative analyses of seven technologies to facilitate the integration of fluctuating renewable energy sources. IET Renew. Power Gener. **3**(2), 190–204 (2009)
15. Takahashi, R., Kinoshita, H., Murata, T., et al.: Output power smoothing and hydrogen production by using variable speed wind generators'. IEEE Trans. Ind. Electron. **57**(2), 485–493 (2010)
16. Bragard, M., Soltau, N., Thomas, S., De Doncker, R.W.: The balance of renewable sources and user demands in grids: power electronics for modular battery energy storage systems. IEEE Trans. Power Electron. **25**(12), 3049–3056 (2010)
17. Bhuiyan, F.A., Yazdani, A.: Reliability assessment of a wind-power system with integrated energy storage. IET Renew. Power Gener. **4**(3), 211–220 (2010)
18. Sen, P.C., Ma, K.H.J.: Constant torque operation of induction motor using chopper in rotor circuit. IEEE Trans. Ind. Appl. **14**(5), 1226–1229 (1978)
19. Geng, H., Yang, G.: Robust pitch controller for output power leveling of variable-speed variable-pitch wind turbine generator systems. IET Renew. Power Gener. **3**(2), 168–179 (2009)